Structural Health Monitoring of Industrial Piping Systems

Using Guided Elastic Waves

F. Schubert, B. Frankenstein, D. Hentschel, K.-J. Fröhlich, M. Küttner, B. Lamek,
Fraunhofer Institute for Nondestructive Testing (IZFP), Dresden Branch, Germany
J. Schwenkkros, DOW Stade, Germany
K. Kerkhof, MPA Universität Stuttgart, Germany
R. Petricevic, Neue Materialien Würzburg GmbH, Germany

Abstract. Guided elastic waves in the frequency range of a few hundred kHz, generated and detected by appropriate transducer arrays, are used to monitor the structural integrity of pipes by comparing their actual state with a predefined reference state. For these purposes, theoretical, numerical, and experimental results are combined to study guided wave propagation and wave interaction with relevant defects in detail. Based on these findings, a guided wave based multi-channel structural health monitoring (SHM) system is designed and applied to identify and monitor structural defects in various piping components. The potential use of synthetic aperture techniques is discussed yielding spatial distributions of damage parameters along the pipe. The results reveal that guided wave based SHM in the kHz frequency regime has great potential for online monitoring of piping systems. It combines imaging techniques with long range detection capabilities and therefore closes the gap between local high-frequency NDE on the one hand and global low-frequency vibration analysis on the other hand.

Keywords. Guided elastic waves, Structural health monitoring (SHM), Piping systems

INTRODUCTION

Many pipes and piping systems are partly or totally inaccessible from the outside, e.g. by being isolated, lying underwater, or being buried in soil. Therefore, it is not possible to detect defects like cracks or corrosion without removing the isolation or uncovering the pipe itself which is very costly and in many cases utterly impossible. For these kinds of problems long-range inspection systems are needed. For corrosion testing of areas of light poles and pipes ultrasonic based testing systems are already available (e.g. [1-3]). However, the systems in their present form are not very well suited for SHM purposes due to size and costs. In order to cover a complete industrial plant with a large number of transducer units, new approaches for measurement hardware, sensor technology, and data evaluation are necessary. This is one of the main goals of the ongoing European SAFE PIPES project. First results of this work are presented in the following together with some basics of guided wave propagation in pipes.

1. STRUCTURAL HEALTH MONITORING USING GUIDED ELASTIC WAVES

Traditional vibration-based monitoring techniques provide global information on a structure under investigation by identifying and analyzing specific resonance modes and by characterizing the condition of mountings and dampers. Due to the low frequencies only large struc-

tural defects can be identified and moreover, cannot be precisely localized in general. For crucial error-prone parts of a structure, vibration monitoring can be efficiently supplemented by using elastic waves in the kHz frequency regime. These ultrasonic waves have a shorter range but are more sensitive to smaller defects and thus, can serve as an early-warning system raising an alarm long before critical damage occurs. If the wavelengths are comparable with or larger than typical dimensions of the structure (e.g. thickness), the waves are called "guided waves". In this case geometrical dispersion cannot be neglected in general (see e.g. [4]).

If using elastic waves for structural health monitoring (SHM) purposes two different approaches are possible, a passive and an active approach. In a passive SHM system, only sensors are needed and "natural" sources like ambient vibrations or acoustic emission (AE) caused by crack generation and growth are detected. Distinct AE events can be localized and characterized and can also be used for imaging purposes using acoustic emission tomography [5]. In an active SHM system the transducers are acting as both, sensors and actuators. By using pulse-echo or acoustic signature techniques, scattered waves from inside the structure or changes in acoustic signature response can be detected and used as damage indicator. A set of transducers spans a so-called 'synthetic aperture'. By temporally delayed excitation and detection of individual actuators and sensors, elastodynamic wave fields can be focused to specific control volumes of the structure which serves as a basis for powerful SHM imaging techniques.

In order to implement a monitoring system based on guided waves, the theoretical fundamentals of guided wave propagation in various structures and their interaction with potential defects have to be investigated first. This can be done via numerical simulation or laser detection of elastic wave fields at the surface of the structure.

The simplest case of guided waves can be found in plate-like structures where so-called 'plate waves' or 'Lamb waves' exist. In general, symmetric and antisymmetric wave modes are being distinguished. They are dispersive in general. In most cases, SHM techniques are working in the low-frequency regime below 500 kHz and thus, only the 0^{th} order Lamb waves are of particular interest for monitoring applications. In addition to the Lamb waves, also horizontally polarized shear waves (SH waves) can be used. In contrast to the Lamb waves the 0^{th} order SH wave is non-dispersive. Numerical and experimental investigations show that each wave mode mentioned above shows different sensitivity to specific kinds of damage. The SH0 mode is well-suited for crack detection and for any application where a surrounding fluid limits the range of the other modes. A0 is best suited for determination of delaminations and local changes in wall thickness. S0 is suited for crack detection and is used in cases, where first-arrival time picking together with a clear identification of the incoming wave is necessary.

The main difference between a pipe and a plate is the curvature of the pipe producing additional dispersion effects. We calculated phase and group velocity diagrams for our laboratory demonstrator, a free 3 m long steel pipe with a diameter of 406 mm and a wall thickness of 9 mm. The corresponding phase velocity diagram calculated by the approximate shell theory of Mirsky and Herrmann [6] is shown in Fig. 1. In this approximation the dispersion of the L(0,2)/F(x,3) (or "P-S0") modes arising at higher frequencies is not included. Moreover, only the first five basic modes are covered.

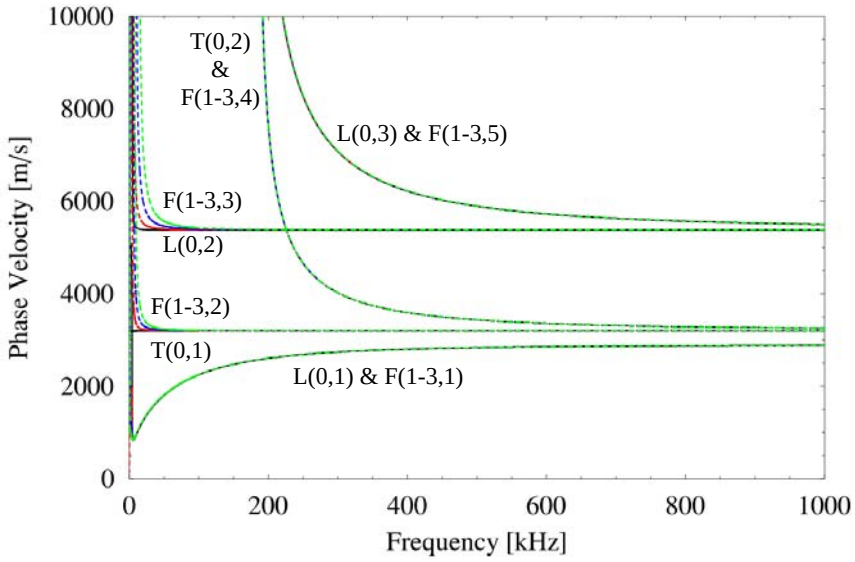

Figure 1: Phase velocity as a function of frequency for various guided wave modes in a free steel pipe with a diameter of 406 mm and a wall thickness of 9 mm. The frequency band between 50 and 200 kHz seems to be most appropriate for long-range SHM applications since in this region only a limited number of wave modes is available and can be easily separated if necessary.

In guided wave theory of cylindrical shells, the following naming convention for the different wave modes is commonly used:

1. **Longitudinal** modes are named **L(0,m)** with n = 0 indicating an **axisymmetric** mode and m = 1,2,… indicating modes of order 1,2, etc.
2. **Torsional** modes are named **T(0,m)** with n = 0 indicating an **axisymmetric** mode and m = 1,2,… indicating modes of order 1,2, etc.
3. **Flexural** modes are named **F(n,m)** indicating **non-axisymmetric** modes with n, m = 1,2, etc.

One can see from Fig. 1 that many wave modes are degenerated in certain frequency bands, i.e. their dispersion curves are identical. For example L(0,2) cannot be distinguished from F(1-3,3) for frequencies > 130 kHz, or T(0,2) has the same dispersion characteristic than F(1-3,4), at least in the velocity-frequency window shown here.

The degeneration of wave modes as explained above simplifies the situation for f > 100 kHz significantly, since only a limited number of wave modes (3-5) instead of dozens of different modes have to be taken into account. In this frequency regime the curves are very similar to the dispersion diagrams of a plate. Up to a certain frequency threshold (here at approx. 180-200 kHz) only three wave modes are present, L(0,1), L(0,2), and T(0,1). Their degenerated flexural counterparts are F(1-3,1), F(1-3,3), and F(1-3,2). These basic pipe modes can be associated with the fundamental plate modes, i.e. the fast symmetric and weakly dispersive S0 mode (≅ L(0,2)), the slow antisymmetric and dispersive A0 mode (≅ L(0,1)), and the non-dispersive SH wave (≅ T(0,1)). Above the frequency threshold mentioned above, higher order modes arise (T(0,2) and L(0,3) in this case), similar to plate diagrams.

Besides these similarities between plate and pipe, there are also significant differences arising in the low-frequency region of the dispersion diagrams, where the degeneration of the wave modes is abrogated and a large number of different modes is present. This is the central

difference to the plate dispersion. While in a free plate things become easy and clear at low frequencies, the situation in a free pipe becomes difficult and more complex. The main consequence of these results is that in order to avoid the confusing influence of higher-order modes in the pipe, it is reasonable to use the relatively small frequency band between 50 and 200 kHz for long-range SHM purposes. Only in this regime wave propagation seems to be manageable and the number of modes is reduced to the three fundamental modes that can be directly associated with the S0, A0, and SH modes in a plate. For the sake of simplicity and clarity we will call these modes 'pipe-S0', 'pipe-A0', and 'pipe-SH' or shorter, P-S0, P-A0, and P-SH in the following although this procedure is not quite correct formally.

Another peculiarity of wave propagation in a pipe is that waves generated by point-like sources are propagating along a helical curve around the longitudinal axis. This is shown in Fig. 2, where the transient wave field due to a point impact on the outer pipe surface was calculated by using the numerical 3-D CEFIT technique [7]. As a consequence of helical wave propagation, one and the same wave mode can be detected several times at a certain sensor position since different travel paths from the source to the sensor are possible.

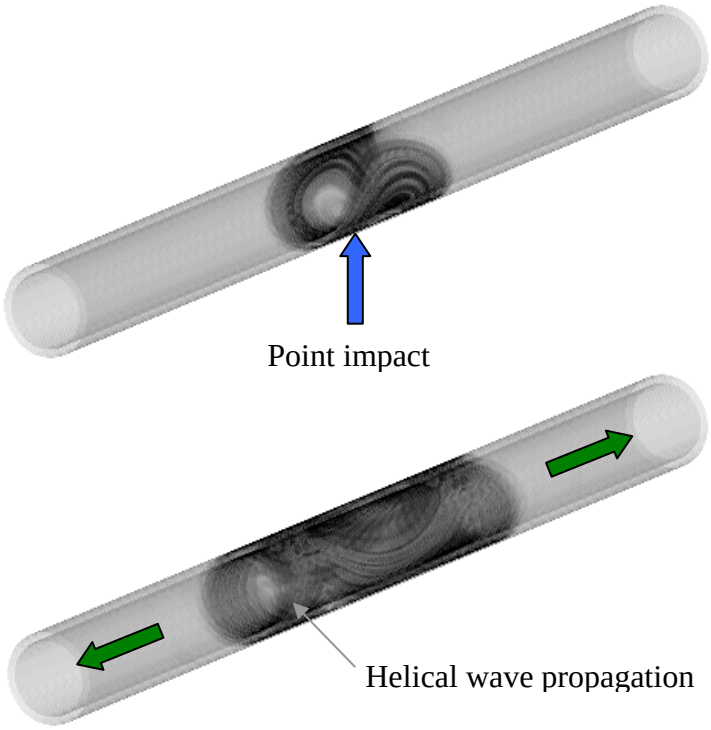

Figure 2: Guided elastic wave propagation in a steel pipe generated by a mechanical radial force point impact on the outer surface of the pipe. The wave front pictures were calculated by using the 3-D elastodynamic finite integration technique in cylindrical coordinates (CEFIT [7]) and show the helical nature of the elastic wave field. Further interesting numerical and analytical investigations of guided waves in free pipes can be found in [8, 9].

In order to verify the theoretical and numerical results from above, various measurements were performed using the laboratory set-up shown in Fig. 3. Rickers wavelets with center frequencies of 70, 126, 240, and 370 kHz were used as excitation signals. The detected waveforms at a sensor position lying 150 cm away from the source are given in Fig. 4. It should be noted that the time axis is given with a constant offset of +68 µs, i.e. the arrival times have to be corrected for that value before calculating the corresponding wave speeds.

Figure 3: Steel pipe as used for the laboratory measurements (length = 3 m, diameter = 406 mm, wall thickness = 9 mm, top picture). Depending on the temperature of the pipe and the intended wave mode used for monitoring, different kinds of transducers based on PZT ceramics, langasite crystals or EMAT technology can be used. In the present case, PZT fibre transducers provided by project partner NMW are glued to the outer pipe surface (bottom pictures). These transducers are characterized by a preferential directivity along the pipe axis and can be used for low-temperature applications up to 80° C and for frequencies up to 600 kHz.

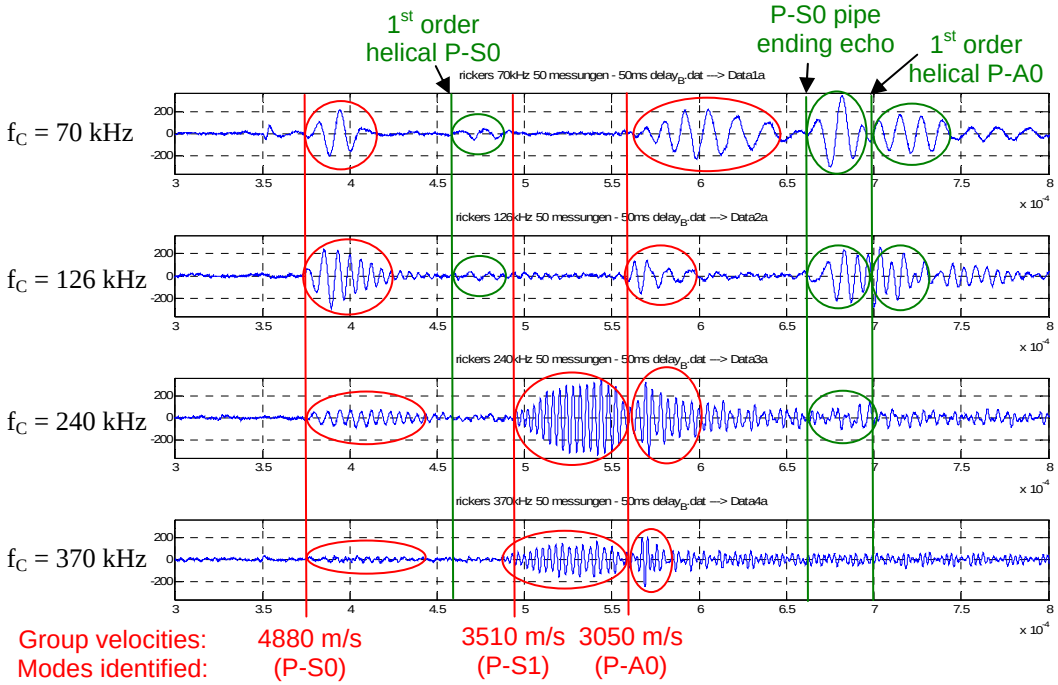

Figure 4: Measured time-domain signals along the steel pipe for four different center frequencies of the input pulse. All elementary wave modes as predicted by theoretical and numerical investigations (including helical modes) could be identified.

In Fig. 4, the first arrival at t ≈ 375 µs (–68 µs offset) is due to the fastest wave mode present, i.e. the P-S0 mode (or F(1,3)). The second elementary wave mode in the first two rows of Fig. 5 arrives at t ≈ 560 µs (–68 µs offset) and can be associated with the P-A0 mode (or F(1,1)). If the center frequency of the input pulse is increased to 240 kHz, a new wave mode suddenly occurs. It is strongly dispersive and - due to its group velocity - can be identified as the first higher-order symmetric mode P-S1 (or F(1,5)).

Besides the primary wave modes, indicated by red ellipses in Fig. 4, also secondary wave modes appear. The latter are indicated by green ellipses. At about 460 µs (–68 µs offset) a wave mode appears at 70 and 126 kHz that is in line with the 1st order helical P-S0 mode whose travel distance between source and receiver is approx. 2 m instead of 1.5 m for the direct wave. The same effect can be observed for the P-A0 mode whose 1st order helical counterpart arrives at approx. 700 µs (–68 µs offset). In both cases, the signal shape of direct and helical wave is similar but the amplitude of the helical wave is smaller due to the larger geometrical spreading along the longer propagation path.

Another interesting echo can be found at 665 µs (–68 µs offset). Since the distance between each of the two transducers to the nearest pipe ending was 75 cm, a wave reflected at the pipe endings reaches the sensor after a propagation path of 3 m. Thus, the wave described above can be identified as the P-S0 echo of the pipe ending. Due to reflection at the free end and the fact that two different propagation paths with identical length contribute to the signal (‘actuator → right pipe ending → sensor’ and ‘actuator → left pipe ending → sensor’), the amplitude of the echo is larger than the amplitude of the primary wave.

As a summary one can conclude that the measurement results are in a good agreement with the theoretical and numerical findings since all existent wave forms in Fig. 4, even the secondary helical waves and pipe ending echoes could be identified. It is worth mentioning that the single PZT fibre actuator used for the measurement produces both, P-S0 and P-A0 modes but no (significant) P-SH mode.

2. DIRECTIVITY PATTERN OF GUIDED WAVES ALONG A STRAIGHT PIPE

Since the monitoring system is using a number of distributed transducers, it is important to study the directivity characteristic of group velocities and damping coefficients of the different wave modes generated by a single transducer. For this purpose the measurement set-up shown in Fig. 5 was used. The sensor on the left was shifted along the black curved line in steps of 2°. Each point on the line has the same geometrical distance of 50 cm to the source position. A 130 kHz RC4 signal was used as input pulse. The results for angle-dependent group velocity and damping coefficient for P-S0 and P-A0 modes are given in Fig. 6.

The group velocity of the P-S0 mode in the top picture of Fig. 6 varies between 4400 and 5200 m/s with a mean value of about 4800 m/s. Thus, with an accuracy of ± 8%, the P-S0 group velocity can be seen as constant for each propagation direction. The P-A0 group velocity fluctuates between 2800 and 3300 m/s with a mean value of about 3100 m/s. With an accuracy of ± 10%, the P-A0 group velocity can also be seen as constant for each propagation direction. This experimental finding is very important for any SHM based imaging or localization technique where group velocities in various propagation directions are needed for reconstruction.

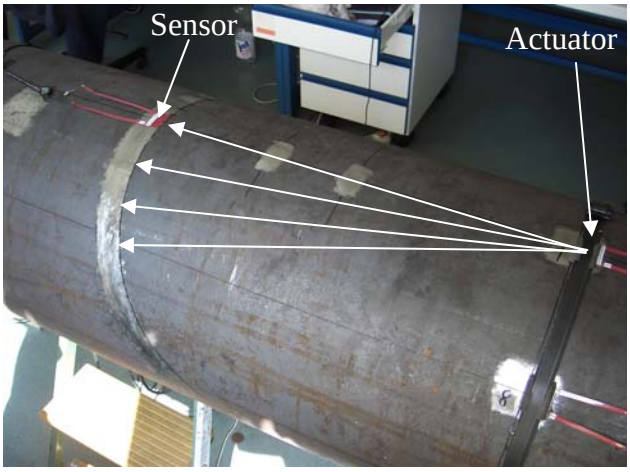

Figure 5: Experimental set-up as used for the measurement of the directivity patterns of P-S0 and P-A0 modes generated by a piezo fibre transducer. The sensor on the opposite side was shifted along the curved black line. Each point on the line has the same geometrical distance of 50 cm to the source position.

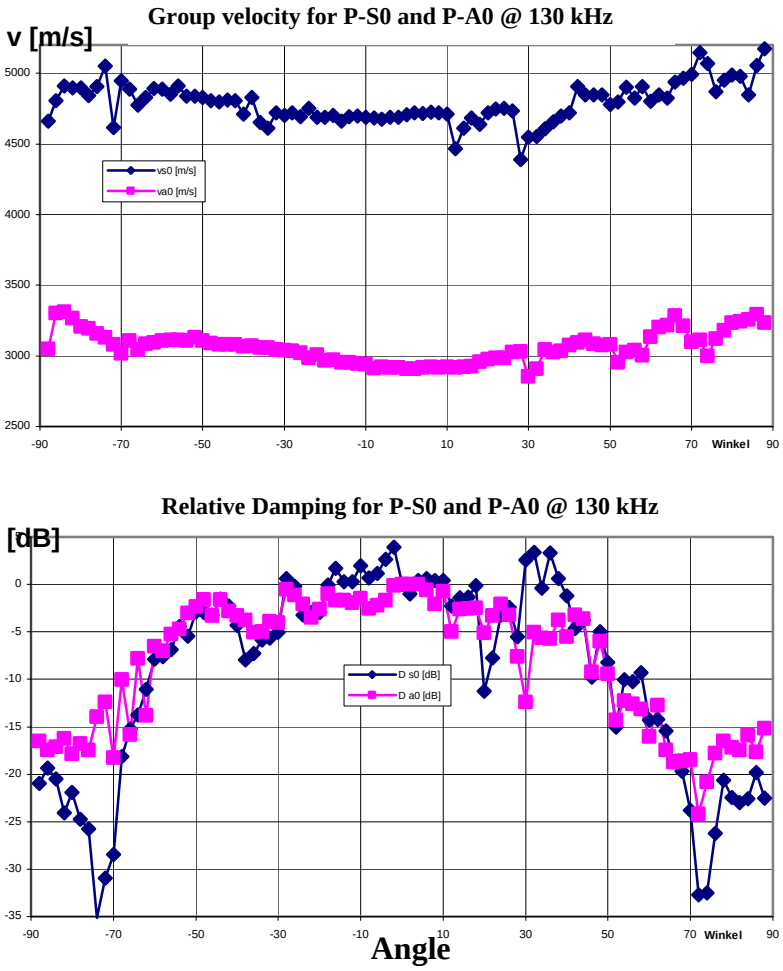

Figure 6: Experimental results for angle-dependent group velocity and damping coefficient for P-S0 (dark blue) and P-A0 mode (magenta) at a center frequency of 130 kHz. The group velocities can be seen as roughly constant in each direction. With the exception of large angles >70° the relative damping coefficients for P-S0 and P-A0 are similar to each other. For the range between ± 50° a damping of only 5-10 dB is obtained.

The angle-dependent damping coefficient, as given in the bottom picture of Fig. 6, shows a similar behavior for the P-S0 and P-A0 mode. Only for large angles above 70°, the relative damping of the P-S0 mode seems to be higher. For the range between ± 50°, a damping of only 5-10 dB is obtained for each wave. That means that at 130 kHz the fibre transducer generates a relatively wide beam of guided waves with a good acoustic coverage of the pipe area to be monitored. Further investigations using a steel pipe mock-up of MPA revealed that with appropriate pre-amplification propagation distances of more than 10 m are manageable.

3. INTERACTION OF GUIDED WAVES WITH DEFECTS

The interaction of elastic waves with structure-relevant defects represents the most important aspect of guided wave based monitoring systems. In general one can say that the higher the frequency the better the spatial and temporal resolution of the monitoring system and the better the sensitivity to small defects. However, for high frequencies the number of existing wave modes is increased and strong dispersion leads to a complex situation and a severely limited range. The lower the frequency the smaller the number of wave modes (at least in plates) and the larger the obtainable range. However, these advantages are cancelled by a significantly lower sensitivity to small defects. Therefore, to choose a specific frequency for the input pulse always means to make a compromise between flaw sensitivity on the one hand and obtainable range and dispersion of the corresponding wave modes on the other hand. If using traditional ultrasonic NDE systems working in the MHz frequency regime, very small cracks in the µm range can be found but the structural information is usually limited to a small area of the pipe. If the whole pipe must be tested, an appropriate scanning device is necessary.

In guided wave based SHM, a larger part of the pipe can be examined within one measurement cycle. Due to the fact that monitoring can be performed in nearly arbitrary time intervals of a few seconds up to a few days, the critical size of defects that have to be found can be increased compared to traditional NDE which usually is applied in periodic intervals of months or years. Statements from industrial partners DOW and RWE revealed that in a typical pipe, crack-like defects not larger than three times the wall thickness and not deeper than 1/3 to 1/2 of the wall thickness have to be found by an SHM system. For the steel pipe described in the previous sections (wall thickness = 9 mm) this means that the monitoring system must be able to find cracks not larger than 27 mm and not deeper than 3-4.5 mm. As a rough rule of thumb one can say that a defect becomes detectable if its lateral size is at least comparable to the wavelength of the specific wave mode used for the measurements and if its depth is larger than 10-15% of the wall thickness. According to this rule, guided waves in the frequency range between 100 and 200 kHz with wavelengths between 20 and 50 mm as described in the previous sections should be able to meet the requirements of defect sensitivity on the one hand and sufficiently large range on the other hand.

In order to investigate the interaction of guided waves with relevant defects, experimental measurements at the steel pipe using two transducer arrays with 8 PZT fibre transducers in each case were performed. Four transducers at a time were combined to a 4-channel sensor/actuator node as shown in Fig. 7. Each of the 16 transducers can be used as source and receiver. If one transducer is emitting, 16 transducers (including the source) can detect the system response. That means that a total of $8 \times 16 \times 2 = 256$ time-domain signals are available for data evaluation and for synthetic aperture reconstruction. However, in the case presented here only transducers #2 and #4 are involved.

Figure 7: 4-channel sensor/actuator nodes for SHM of piping systems. The nodes can be combined to a multi-channel measuring system (16 channels in this case) that can be used for both active and passive monitoring. The present nodes are based on a CAN bus interface but wireless interfaces are also under development. Details of the hardware implementation can be found in [10].

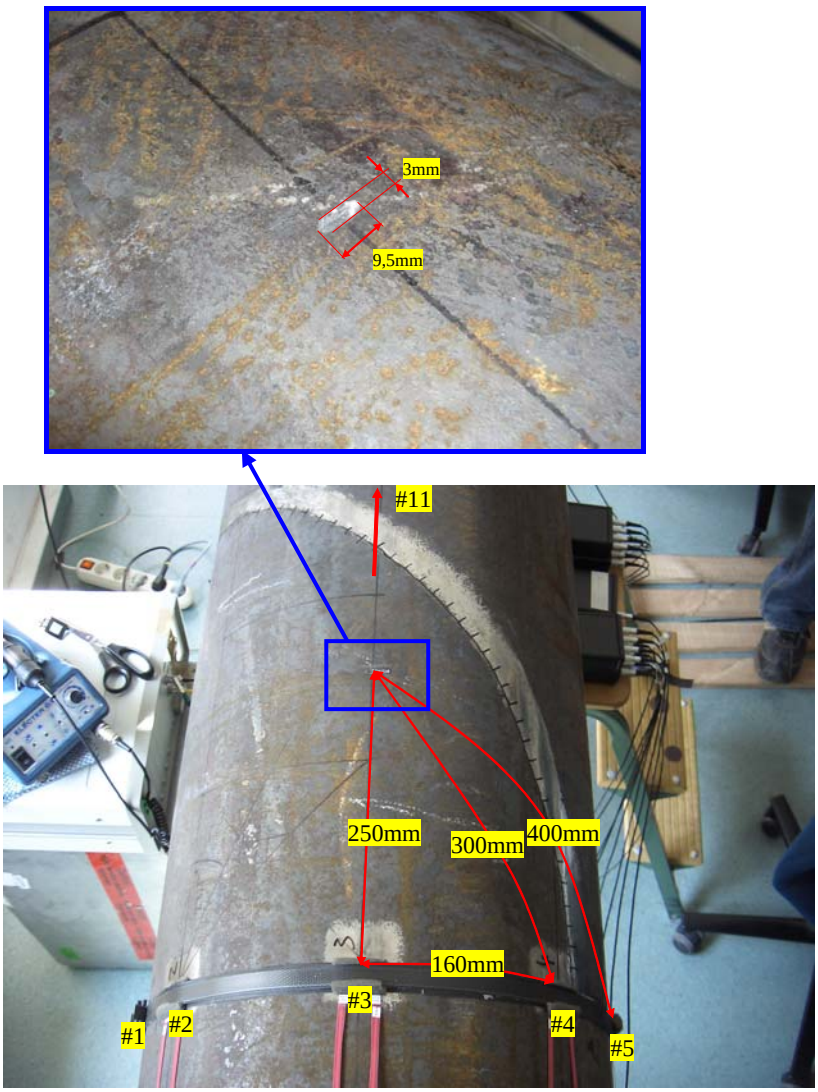

Figure 8: Details of the set-up showing the distance of the notch to the relevant transducers. For the measurements shown in the following Fig. 9, transducers #2 and #4 were used.

9.5 mm notch

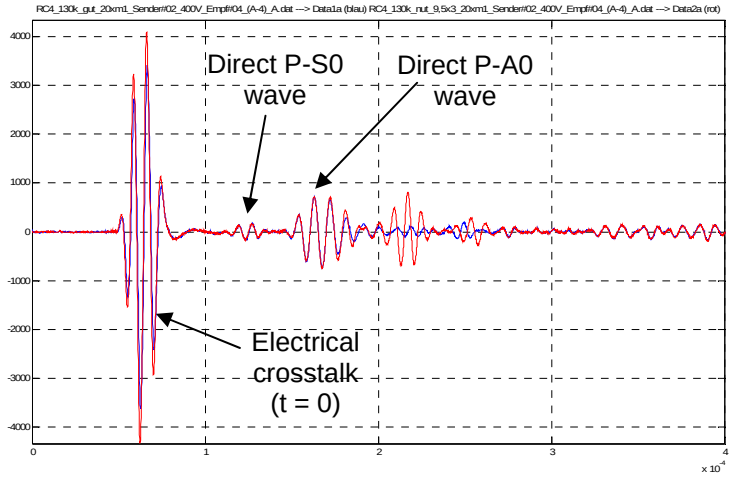

19 mm notch

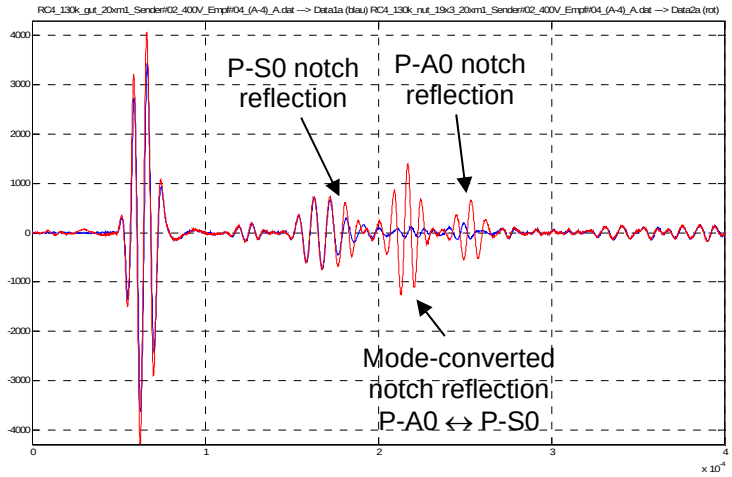

27 mm notch

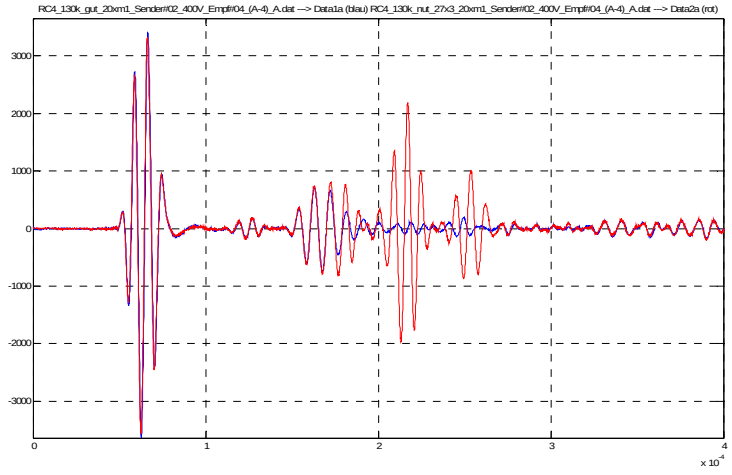

Figure 9: Results for three different notches (red curves) using transducer #2 as actuator and #4 as sensor. The blue curve represents the reference measurement (baseline) without notch.

A notch lying perpendicular to the longitudinal axis of the pipe was artificially inserted along the connecting line between transducers #3 and #11 in a distance of 25 cm to transducer #3

and 30 cm to transducers #2 and #4, respectively. The notch was enlarged in two steps so that all in all three notch sizes were available for the measurements. In each case the width and depth of the notch was 3 mm, the length varied from 9.5 mm over 19 mm up to 27 mm. The details of the set-up including the relevant distances to the notch are given in Fig. 8.

For the measurements, an RC4 input pulse with a center frequency of 130 kHz was used. The main idea of the underlying SHM system is the comparison of the actual state of the pipe with a certain reference state ("baseline approach"). This reference state can either be the pipe without any defects or alternatively, a state with smaller defect size. For the present investigation, a reference measurement without any defects was performed first. After that the measurements including the defects were done and compared to the reference state.

Figure 9 shows the time-domain signals for the measurements at the three different notches using transducer #2 as source and #4 as receiver (red curves). In this case a specular reflection of the waves at the notch can be expected. For better comparison, the result for the reference measurement without notch is also given in each case (blue curve). The first strong signal at about 50 µs is an electrical crosstalk which serves as the temporal origin, $t = 0$. At about 117 µs (i.e. 67 µs after the crosstalk) a weak contribution appears that can be associated with a direct circumferential P-S0 wave between source and receiver. The direct P-A0 wave is expected at 160 µs (i.e. 110 µs after the crosstalk) and is really found there. Its amplitude is stronger than the direct P-S0 wave which is in accordance with the angle-dependent damping curve in Fig. 6. These direct signals are expected to remain constant for increasing notch size and in fact this can be observed for both modes.

At about 175 µs (i.e. 125 µs after crosstalk), the signal becomes slightly higher than the reference signal. Due to the arrival time it can be identified as the P-S0 notch reflection although its contribution is partly superimposed by the direct P-A0 wave. This signal is only slightly increasing with increasing notch size, revealing that the P-S0 interaction with the notch is rather weak. At about 200 µs (i.e. 150 µs after the crosstalk) a strong signal appears that can be associated with a mode converted notch reflection whereas the incident P-A0 mode is converted into a P-S0 wave during the scattering process. In principle also the inverse procedure, i.e. mode conversion from incident P-S0 to P-A0 wave is possible since the arrival time is the same. This mode-converted echo leads to a significant deviation from the reference curve, even for the small notch. With increasing notch size, the echo is also increased showing a nearly linear relationship between notch size and echo amplitude.

At approx. 245 µs (i.e. 195 µs after crosstalk) the direct P-A0 echo from the notch arrives. This echo is also strongly increased with increasing notch size and thus also serves as a sensitive indicator for the notch growth. It is remarkable that the mode-converted notch echo is larger than the pure P-A0 echo by roughly a factor of two.

Beside the measurement described above various other measurements with other source-receiver combinations were performed and also the forward scattered field was studied. As a conclusion from these measurements one can summarize that the changes in the backward scattered field are by far more significant than the changes in the forward scattered field. However, the changes in the backward field are surprisingly strong, although the size of the notch was smaller than the wavelengths of the wave modes involved and the depth of the notch was only 1/3 of the wall thickness.

In Fig. 9 the interaction of guided waves with the artificial notches is well-defined and the resulting echoes are strong and can easily be associated with specific wave modes and mode-converted echoes. However, in more realistic structures with complex geometry like the Titanium elbow shown in Fig. 10, the wave/defect interactions are more difficult and subtle so that more pragmatic and robust data evaluation schemes have to be used.

Figure 10: Titanium elbow (wall thickness = 6 mm) with notches artificially introduced into a weld seam. The notch depth was varied between 1 mm (first step) and 5.3 mm (last step). Due to the sawing the initial notch length of approx. 12 mm was also increased stepwise.

In one of the weld seams of the elbow artificial notches were inserted by sawing. The depth of the notch was increased from 1 mm up to 5.3 mm in discrete steps. Due to the sawing the length of the notch was also increased simultaneously from approx. 12 mm to 35 mm. For each state the system response of the elbow due to pulse excitation was determined for different actuator/sensor combinations and was compared with a reference state without defects.

Fig. 11 shows typical time-domain signals along path A-D_1, i.e. transducer A serves as actuator and transducer D_1 as sensor (compare Fig. 10). The center frequency of the input pulse was f = 150 kHz in this case. For the 1 mm deep notch, the difference to the reference measurement without notch is rather small and thus, the linear correlation coefficient between both curves is nearly equal to one. For the 3.5 mm notch the difference between the curves is significantly larger and therefore, the correlation coefficient drops to approx. 0.97. For calculation of the correlation coefficients we used the Hilbert envelope of the signals instead of the signals themselves due to higher robustness.

The measurements were repeated for different notch depths and various center frequencies of the input pulse as well as for different propagation paths. In Fig. 12 the results of the correlation analysis are displayed for propagation paths A-D_1 and A-D_2 (compare Fig. 10), for notch depths of 1, 2, 3.5, and 5.3 mm, and for frequencies of 150, 200, 250, and 325 kHz, respectively.

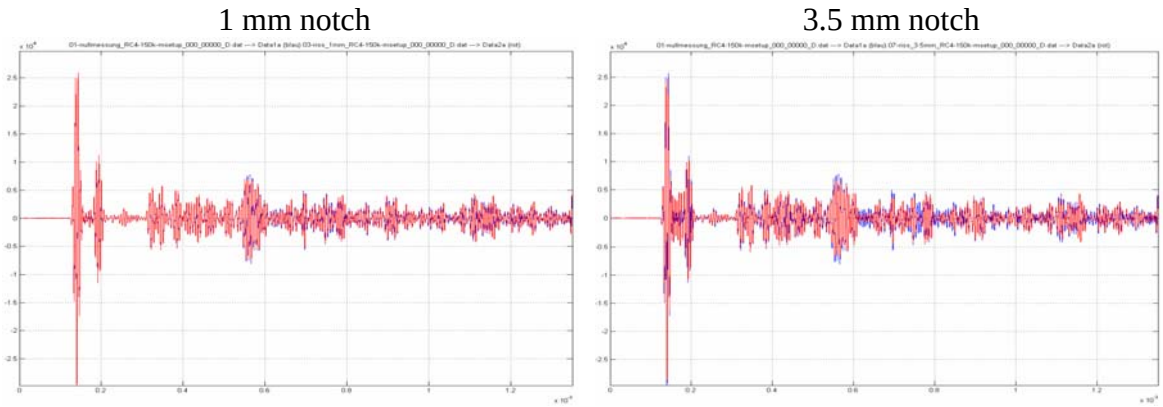

Figure 11: Typical guided wave system response of the Titanium elbow along path A-D_1 for the 1 mm and 3.5 mm deep notch, respectively. Red curves: reference state without notch; blue curves: elbow with notch.

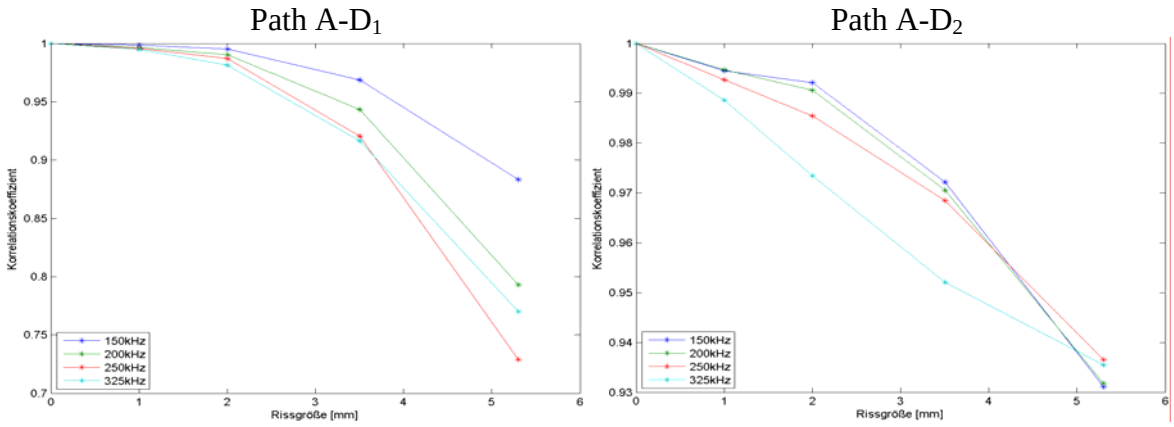

Figure 12: Correlation coefficients as a function of notch depth (horizontal axis) and center frequency of the input pulse (coloured curves) for propagation paths A-D_1 and A-D_2, obtained by comparing the particular Hilbert envelope of the time-domain response at sensor D with the reference measurement without notch. As a general trend the correlation coefficient decreases with increasing notch depth and increasing frequency and thus serves as a sensitive damage indicator even for the long propagation path A-D_2.

As a general trend we find that the correlation coefficient decreases with increasing notch depth and also with increasing frequency. These results are physically plausible since in both cases the interaction between guided waves and the defect is enlarged. For the short propagation path A-D_1 the overall drop of the correlation coefficient is to values between 0.88 and 0.73. For the longer path A-D_2 the overall drop is only to values between 0.931 and 0.937 but still significant, even for the lowest frequency.

The results revealed that under laboratory conditions crack-like defects having a depth of only 1/5 of the wall thickness can be detected by such a monitoring system even in complex geometries with flanges, weld seams, and curvatures, and in cases where the wavelengths are not significantly larger than the lateral size of the defect and where the distance to source and receiver is rather large.

In field tests a worse signal-to-noise ratio can be expected due to background noise and other disturbances. However, due to the fact that the coupling conditions remain constant and the excitation is reproducible, the measurements can be repeated many times in order to increase the signal-to-noise ratio until it reaches an acceptable level.

4. GENERAL CONCEPTION OF THE SHM SYSTEM

The general conception of the SHM system is shown in Figs. 13 and 14.

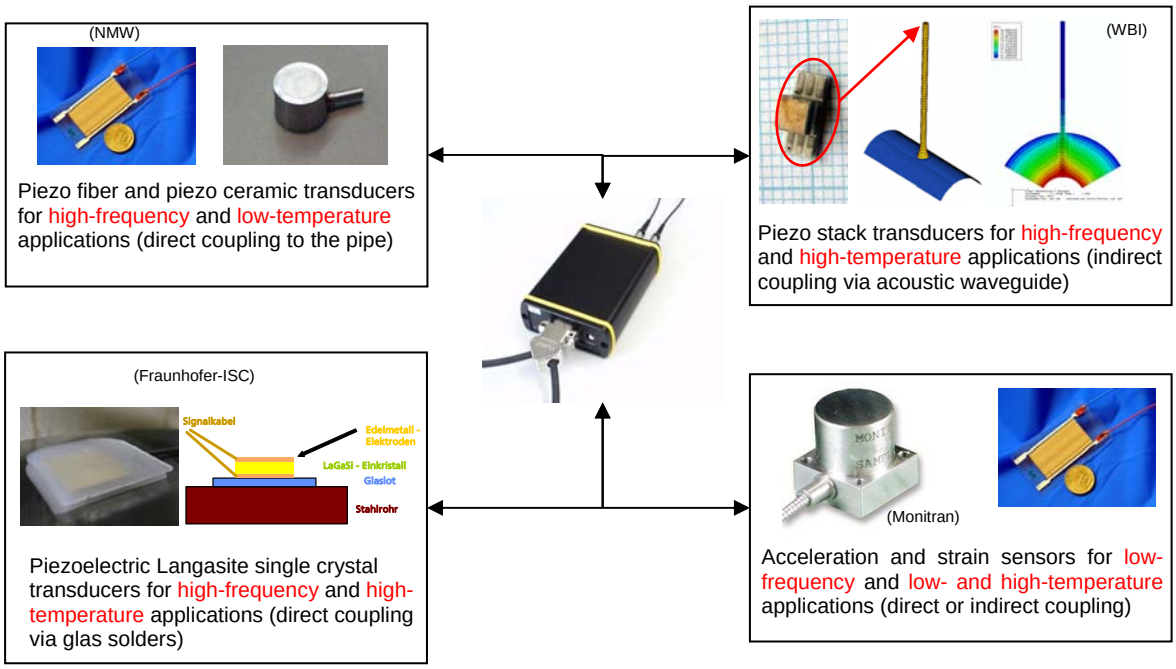

Figure 13: Conception of the modular transducer system. The SHM network will be able to manage different kinds of transducers and sensors for low- and high-temperature applications and for low- and high-frequency monitoring.

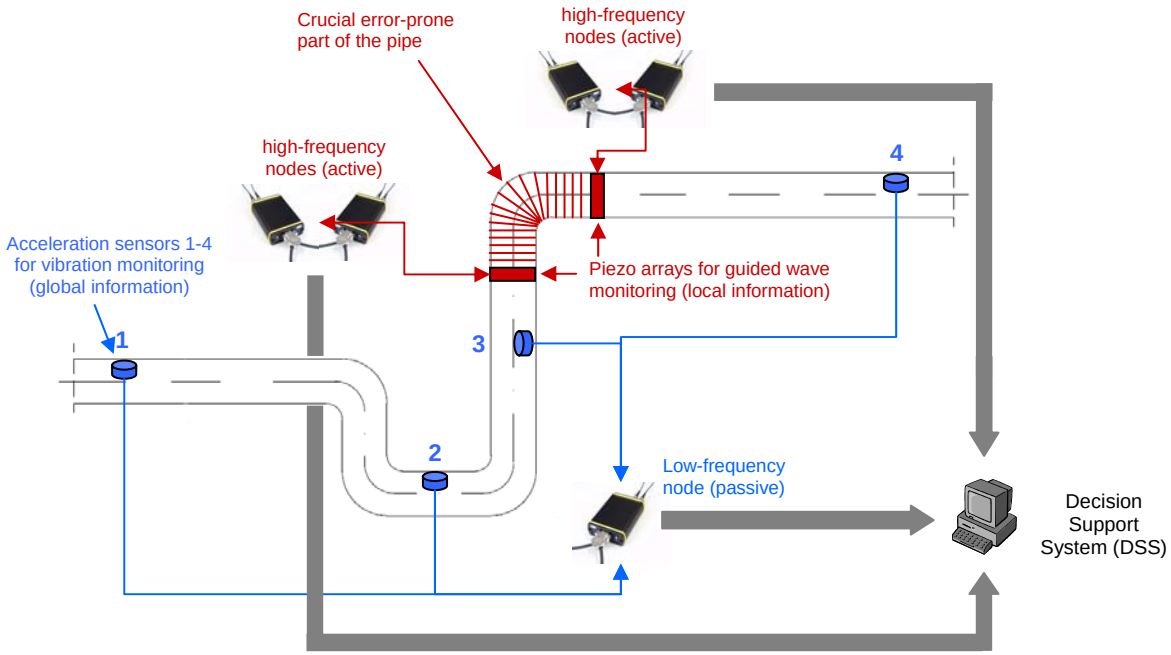

Figure 14: Combination of low- and high-frequency monitoring. Wile the passive low-frequency nodes with acceleration and strain sensors are responsible for global vibration monitoring of the structure (providing information on basic boundary conditions caused by hangers and dampers) the active high-frequency guided wave nodes are used to monitor local crucial and error-prone parts of the piping system.

Each single network node represents a four-channel monitoring system which is able to manage different kinds of actuators and/or sensors. Two different types of nodes are available, one for high-frequency guided wave monitoring and another type for low-frequency vibration monitoring. Each single node can be combined with several others resulting in a multi-channel monitoring system. Various transducers for low- and high-temperature applications and for low- and high-frequency monitoring can be used as exemplary demonstrated in Fig. 13.

However, the key concept of the proposed approach is the combination of low- and high-frequency monitoring as shown in Fig. 14. Wile the passive low-frequency nodes with acceleration and strain sensors are responsible for global vibration monitoring of the structure (providing information on basic boundary conditions caused by hangers and dampers) the active high-frequency guided wave nodes are used to monitor local crucial and error-prone parts of the piping system. Both levels, i.e. local and global ones, will be combined adaptively dependent on the actual state of the piping system. The monitoring results from both types of nodes will finally merge in a joint decision support system (DSS) based on case based reasoning or other learning approaches. This DSS is still under development.

5. CONCLUSIONS AND OUTLOOK

The results obtained so far clearly show that guided elastic waves in the frequency range between 70 and 350 kHz are well-suited for determination of pipe defects having dimensions as specified by the industrial partners. The existent wave modes can be clearly identified by using theoretical and numerical models and thus, the monitoring system can be adjusted and optimized to the specific pipe geometry and to the kind of defect to be identified.

It can therefore be expected that a guided wave based SHM system is able to efficiently close the gap between high-frequency NDE in the MHz frequency regime on the one hand and low-frequency vibration analysis on the other hand. The goals of an overall monitoring system that combines low- and high-frequency data can be summarized as follows (with increasing level of complexity):

1. Identification of defects: Raise an alarm if a defect is present
2. Localization of defects: If a defect is present, determine its (approximate) position
3. Relevance of defects: State if the defect is relevant for the structural integrity of the pipe
4. Residual lifetime: Try to estimate the remaining lifetime of the structure

From our point of view an SHM system based on elastic waves and vibrations is able to contribute to the first and second point in the preceding list at least. To meet these requirements appropriate damage parameters have to be extracted from the detected signals and efficient imaging techniques have to be developed by using synthetic aperture array techniques. These methods have to be robust against specific and irregular boundary conditions, e.g. a fluid loaded pipe instead of a free pipe, turbulent flows inside the pipe etc. These aspects are subjects of ongoing work within the SAFE PIPES project.

ACKNOWLEDGMENT

The present work has been supported by the Commission of the European Communities in the framework of the specific targeted research project SAFE PIPES (Safety Assessment and Lifetime Management of Industrial Piping Systems) under the 6th framework program (NMP2-CT-2005-013898). This support is gratefully acknowledged. We also thank all our partners in the SAFE PIPES consortium, especially NMW Würzburg for providing us with the PZT fibre transducers, and DOW Stade and MPA Stuttgart, respectively, for supply and mechanical preparation of the Titanium elbow. Many thanks also to WBI Höchberg and Fraunhofer-ISC Würzburg for the pictures used in Fig. 13.

REFERENCES

[1] D.N. Alleyne, B. Pavlakovic, M.J.S. Lowe, and P. Cawley, "Rapid long-range inspection of chemical plant pipework using guided waves", Insight, Vol. **43**, No. 2, 93-96, February 2001.

[2] P. Cawley, M.J.S. Lowe, D.N. Alleyne, B. Pavlakovic, and P. Wilcox, "Practical Long Range Guided Wave Testing: Applications to Pipes and Rail", Materials Evaluation, 66-74, January 2003.

[3] H.J. Salzburger, "Long Range UT by Structural Ultrasonic Waves and Electromagnetic Acoustic Transducers (EMAT)", 16th Major International UT conference and Exhibition 5-7 July, 1995, Edinburgh.

[4] B. Köhler, F. Schubert, B. Frankenstein, "Numerical and experimental investigation of Lamb wave excitation, propagation, and detection for structural health monitoring", In: Proc. of the 2nd European Workshop on Structural Health Monitoring 2004, Munich, Germany, July 7-9, Eds.: C. Boller, W. J. Staszewski, 993-1000, 2004.

[5] F. Schubert, "Basic principles of acoustic emission tomography", Journal of Acoustic Emission, Vol. **22**, 147-158, 2004.

[6] K.F. Graff, *Wave motion in elastic solids*, Clarendon Press, Oxford, 1975.

[7] F. Schubert, "Numerical time-domain modeling of linear and nonlinear ultrasonic wave propagation using finite integration techniques – Theory and applications", Ultrasonics **42**, 221-229, 2004.

[8] T. Hayashi and J. L. Rose, "Guided Wave Simulation and Visualization by a Semianalytical Finite Element Method", Materials Evaluation, 75-79, January 2003.

[9] J. Li and J.L. Rose, "Excitation and propagation of non-axisymmetric guided waves in a hollow cylinder", J. Acoust. Soc. Am. **109** (2), 457-464, February 2001.

[10] B. Frankenstein, D. Hentschel, and F. Schubert: "Monitoring Network for SHM in Aircraft Applications", In: Proc. of SPIE conference on Smart Structures & Materials/NDE, 18-22 March 2007, San Diego, USA.

CONTACT ADDRESS

Dr. Frank Schubert
Fraunhofer-Institute for Nondestructive Testing, Dresden Branch (IZFP-D)
Maria-Reiche-Str. 2, D-01109 Dresden, Germany

Phone: ++49 (0) 351 / 88815-523 (or -621)
Email: Frank.Schubert@izfp-d.fraunhofer.de